HHS Public Access

Author manuscript

Small. Author manuscript; available in PMC 2023 May 01.

Published in final edited form as:

Small. 2022 May ; 18(21): e2107714. doi:10.1002/smll.202107714.

Co-electrospun Silk Fibroin and Gelatin Methacryloyl Sheet Seeded with Mesenchymal Stem Cells for Tendon Regeneration

Prof. Yumeng Xue[1],
State Key Laboratory of Solidification Processing, Center for Nano Energy Materials, School of Materials Science and Engineering, Northwestern Polytechnical University, Xi'an, 710072, China

Department of Bioengineering and Center for Minimally Invasive Therapeutics (C-MIT), University of California, Los Angeles, Los Angeles, CA 90095, USA

Frontier Institute of Science and Technology, Xi'an Jiaotong University, Xi'an, 710000, China

Prof. Han-Jun Kim[1],
Department of Bioengineering and Center for Minimally Invasive Therapeutics (C-MIT), University of California, Los Angeles, Los Angeles, CA 90095, USA

Terasaki Institute for Biomedical Innovation, Los Angeles, CA 90064, USA

Dr. Junmin Lee,
Department of Bioengineering and Center for Minimally Invasive Therapeutics (C-MIT), University of California, Los Angeles, Los Angeles, CA 90095, USA

Department of Mechanical Engineering, YONSEI University, Seoul, 03722, South Korea

Terasaki Institute for Biomedical Innovation, Los Angeles, CA 90064, USA

Prof. Yaowen Liu,
Department of Bioengineering and Center for Minimally Invasive Therapeutics (C-MIT), University of California, Los Angeles, Los Angeles, CA 90095, USA

College of Food Science, Sichuan Agricultural University, Yaan, 625014, China

Tyler Hoffman,
Department of Bioengineering and Center for Minimally Invasive Therapeutics (C-MIT), University of California, Los Angeles, Los Angeles, CA 90095, USA

Dr. Yi Chen,
Department of Bioengineering and Center for Minimally Invasive Therapeutics (C-MIT), University of California, Los Angeles, Los Angeles, CA 90095, USA

Xingwu Zhou,
Department of Bioengineering and Center for Minimally Invasive Therapeutics (C-MIT), University of California, Los Angeles, Los Angeles, CA 90095, USA

[*]Corresponding authors: knjulee@jnu.ac.kr (KangJu Lee), khademh@terasaki.org (Ali Khademhosseini).
[1]These authors equally contributed

Supporting Information
Supporting Information is available from the Wiley Online Library or from the author.

The authors have no **competing interests**.

Dr. Wujin Sun,
Department of Bioengineering and Center for Minimally Invasive Therapeutics (C-MIT), University of California, Los Angeles, Los Angeles, CA 90095, USA

Terasaki Institute for Biomedical Innovation, Los Angeles, CA 90064, USA

Dr. Shiming Zhang,
Department of Bioengineering and Center for Minimally Invasive Therapeutics (C-MIT), University of California, Los Angeles, Los Angeles, CA 90095, USA

Terasaki Institute for Biomedical Innovation, Los Angeles, CA 90064, USA

Prof. Hyun-Jong Cho,
College of Pharmacy, Kangwon National University, Chuncheon, 23431, South Korea

Dr. JiYong Lee,
Department of Bioengineering and Center for Minimally Invasive Therapeutics (C-MIT), University of California, Los Angeles, Los Angeles, CA 90095, USA

Department of Mechanical Engineering, YONSEI University, Seoul, 03722, South Korea

Terasaki Institute for Biomedical Innovation, Los Angeles, CA 90064, USA

Prof. Heemin Kang,
Department of Materials Science and Engineering, Korea University, Seoul, 02841, South Korea

Prof. Ryu WonHyoung,
Department of Mechanical Engineering, YONSEI University, Seoul, 03722, South Korea

Prof. Lee Chang-Moon,
Department of Healthcare and Biomedical Engineering, Chonnam National University, Yeosu, 59626, South Korea

Prof. Samad Ahadian,
Department of Bioengineering and Center for Minimally Invasive Therapeutics (C-MIT), University of California, Los Angeles, Los Angeles, CA 90095, USA

Terasaki Institute for Biomedical Innovation, Los Angeles, CA 90064, USA

Prof. Mehmet R. Dokmeci,
Department of Bioengineering and Center for Minimally Invasive Therapeutics (C-MIT), University of California, Los Angeles, Los Angeles, CA 90095, USA

Terasaki Institute for Biomedical Innovation, Los Angeles, CA 90064, USA

Prof. Bo Lei,
Frontier Institute of Science and Technology, Xi'an Jiaotong University, Xi'an, 710000, China

Prof. KangJu Lee[*],
Department of Bioengineering and Center for Minimally Invasive Therapeutics (C-MIT), University of California, Los Angeles, Los Angeles, CA 90095, USA

Department of Healthcare and Biomedical Engineering, Chonnam National University, Yeosu, 59626, South Korea

Terasaki Institute for Biomedical Innovation, Los Angeles, CA 90064, USA

Prof. Ali Khademhosseini*

Department of Bioengineering and Center for Minimally Invasive Therapeutics (C-MIT), University of California, Los Angeles, Los Angeles, CA 90095, USA

Terasaki Institute for Biomedical Innovation, Los Angeles, CA 90064, USA

Abstract

Silk fibroin (SF) is a promising biomaterial for tendon repair, but its relatively rigid mechanical properties and low cell affinity have limited its usefulness and utility in regenerative medicine. Meanwhile, gelatin-based polymers have advantages in cell attachment and tissue remodeling, but have insufficient mechanical strength to regenerate tough tissue such as tendons. Taking these aspects into account, in this study, gelatin methacryloyl (GelMA) was combined with SF to create a mechanically strong and bioactive nanofibrous scaffold (SG). The mechanical properties of SG nanofibers could be flexibly modulated by varying the ratio of SF and GelMA. Compared to SF nanofibers, mesenchymal stem cells (MSCs) seeded on SG fibers with optimal composition (SG7) exhibited enhanced growth, proliferation, vascular endothelial growth factor (VEGF) production and tenogenic gene expression behavior. Conditioned media from MSCs cultured on SG7 scaffolds, compared to MSCs cultured on SF or GelMA alone nanofibers could greatly promote the migration and proliferation of tenocytes. Histological analysis and tenogenesis related immunofluorescence staining indicated SG7 scaffolds demonstrated enhanced in vivo tendon tissue regeneration compared to other groups. Therefore, rational combinations of SF and GelMA hybrid nanofibers may help to improve therapeutic outcomes and address the challenges of tissue-engineered scaffolds for tendon regeneration.

Graphical Abstract

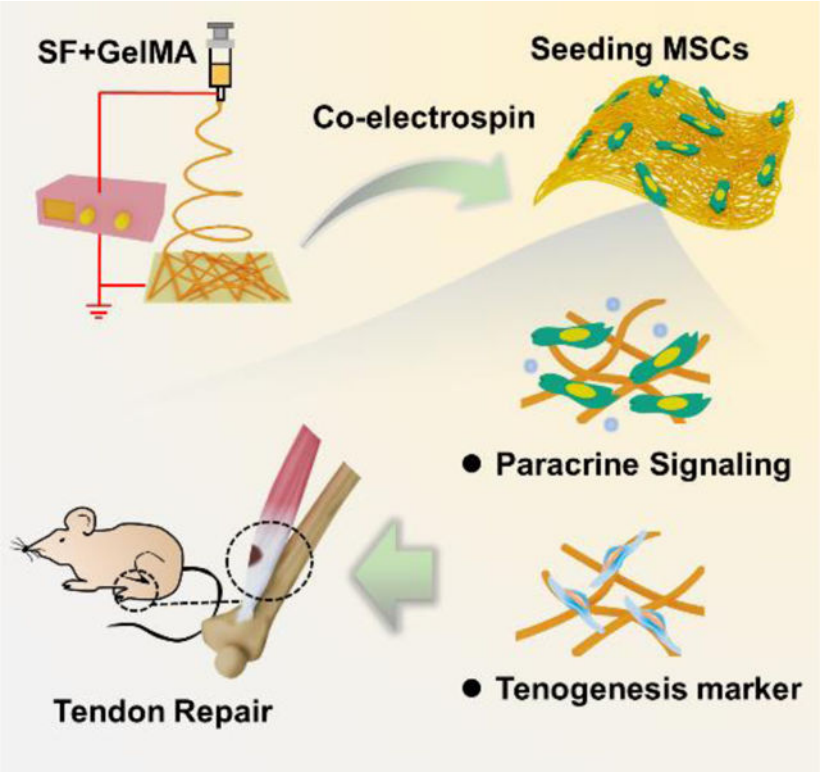

The rationally designed SG hybrid fibrous scaffolds could remarkedly promote tendon tissue regeneration process by mechanically support the growth of MSCs and biologically induce the MSCs proliferation and growth factor secretion, enabling their promising application in tendon tissue repair.

Keywords

electrospinning; gelatin methacryloyl; silk fibroin; mesenchymal stem cell; tendon regeneration

1. Introduction

Tendons are vital tissues that transmit the force between muscle and bone to control body movement [1]. However, during sports or vigorous activities where sudden mechanical load is applied to tissue, tendons can be easily damaged. Tendon tissue repair remains to be a clinical and scientific challenge due to the relatively long rehabilitation time and high failure rates of tissue reconstruction [2]. Following injury, tendon undergoes an endogenous regeneration process which is modulated by short-term inflammation and recruitment of tenocytes and fibroblasts [3]. Due to its physiological and anatomical nature, regeneration processes usually take weeks to months to achieve a functional, stiff extracellular matrix composed of aligned collagen type I fibers [3]. However, inevitable fibrous scars form and remodel during the regeneration process are more likely to exhibit biochemical and biomechanical properties that differ from normal tendons, which may lead to improper

healing after injury and consequently cause constant pain and a decreased quality of life [2b, 4].

For decades, various strategies have been developed to more effectively treat tendon injuries, but it remains difficult to ensure complete functional recovery [5]. Allografts can often result in complications like immune rejection, and autologous transplant run the risk of disease transmission and necrosis of the transplant [6]. The efficacy of synthetic grafts is still limited due to poor mechanical properties, lack of biocompatibility, and biological properties that are not specialized for tendons [7]. Therefore, other treatment methods that are expected to achieve better regeneration, improve the *in situ* tendon reconstruction, and reduce tissue degeneration have been developed for restoring the tendon function. Based on the fact that limited number and low activity/reparative of tendon resident cells are the main culprit which restricted the regenerative capacity of tendons, mesenchymal stem cells (MSCs) mediated cell therapy emerged as a new tendon tissue regeneration strategy has received increasing attention [4b, 8]. The remarkable ability to self-renew, differentiate into various cell lineages, produce abundant functional paracrine factors, shift the balance of regenerative and fibrotic processes of MSCs, combined with the low risk of teratoma formation compared to other stem cells or tissue repair methods, making MSC treatment particularly attractive for tendon repair applications [9].

Examples of the diverse range of MSC treatments for tendon repair include: direct injection or systemic infusion, cell engineering through genetic modifications, and tissue engineering combinations of cells and scaffolds [10]. However, the efficacy of these methods is relatively limited. For instance, cells delivered via systemic infusion usually have poor localization at specific injury sites [8c]. The direct injection of cells requires excessive proliferation to achieve the high cell numbers and the low retention of injected cells may lead to very low functional engraftment yields [9a]. The efficiency of genetically modified stem cells toward the tenogenic lineage is too low [8a]. Therefore, recent attention has shifted to tissue engineering-based strategies where scaffolds are used to deliver MSCs. Although efforts of the last decades aim to achieve a highly efficient and safe tendon injury repair by maximizing the migratory, immunomodulatory, and reparative abilities of MSCs with biomaterials, many issues remain unsolved and the therapeutic efficacy is still unsatisfied toward clinical applications [9b, 11]. For instance, further microstructure and component improvement is needed to achieved favorable local stiffness and microenvironment for MSCs growth [12]. Additionally, poor fixation of scaffolds may lead to complications like synovitis, implant rupture and formation of unwanted tissue over long term [2b]. Moreover, the underlying mechanism of tendon regeneration is unclear in regard to whether MCSs directly differentiate into tenogenic cells or produced cytokines to influence the tendon repair process indirectly [13]. Therefore, we need to rationally develop scaffolds with specific structure and components that can not only provide a microenvironment to mechanically support the in-situ growth of MSCs, but also can effectively induce the biological regeneration ability of MSCs [2b, 14].

To address the above problems, the interactions between the cells and scaffolds within the wound environment must be considered. Ideal scaffolds for tendon repair must be biodegradable, biocompatible, have stiff mechanical properties, exhibit controlled

degradation behavior, and promote native cell migration and proliferation [10a]. Silk fibroin (SF), one of the most popular biocompatible materials, has been widely investigated as a tendon scaffold due to excellent mechanical properties [15]. To further enhanced the tendon regeneration efficacy, combining biomaterials with SF to develop hybrid scaffold with improved mechanical and biological performance was widely investigated [15a]. For instance, the addition of collagen within SF scaffolds could enhance the cell attachment and tendon repair efficacy compared to SF alone [16]. As an alternative, gelatin methacryloyl (GelMA), a popular synthesized biomaterial, exhibits better solubility and less antigenicity compare with collagen and has been widely used in biomedical applications. It has been proven that GelMA supports cell attachment and greatly promotes cell proliferation due to intrinsic arginine-glycine-aspartic acid (RGD) motifs [17]. In addition, GelMA contains matrix metalloproteinase cleavage sites that enables cell-mediated degradation and remodeling of the material. Therefore, in this study, we proposed to co-electrospun GelMA and SF nanofibrous sheet to develop a porous and fibrous sheet, which can improve MSC proliferation and growth factor secretion while maintaining the stiff mechanical properties required for tendon scaffolds (Figure 1). The effect of increasing GelMA content on the chemical and physical properties of nanofibrous sheets was carefully investigated. In addition, we evaluated the influence of SF+GelMA (SG) composite scaffolds on MSC morphology, proliferation, differentiation and cytokines secretion following direct seeding on the nanofiber sheets to figure out the tendon healing mechanism of the SG scaffolds. MSC-seeded SG scaffolds were evaluated for their ability to improve tenocyte migration *in vitro* and improve the extent of tendon regeneration in a mouse tendon injury model.

2. Results and Discussion

2.1. Fabrication and morphology of SG electrospun nanofibers

For co-electrospinning, we first mixed SF and GelMA compounds (SG) in different ratios (SF:GelMA = 15:1, 10:1, 7:1, 5:1, and 3:1 (w/w) and named the electrospun samples SG15, 10, 7, 5, and 3 respectively). Each sample was electrospun at 22 kV (voltage), 0.5 mL/h (feed rate), and 15 cm distance (between the needle and the 100 cm^2 collector). The fiber diameters within the electrospun sheet were measured by scanning electron microscopy (SEM) analysis to characterize the influence of GelMA on the morphology of the fibers. SEM images of the electrospun sheets displayed in Figure 2A–G and Figure S1 demonstrated that changing the SF:GelMA ratio had negligible influence on the morphology of SG fibers. As the amount of GelMA content is increased, SG nanofibers maintained fiber diameter and uniformity. It is worth noting that the GelMA-only fibers showed a similar diameter to SG fibers (Figure S2), but the scaffold did not look as porous. The dense structure of GelMA scaffolds is potentially a result of the crosslinking process, which may result in the shrinkage and reduction in porosity. This phenomenon confirmed that the existence of SF could effectively maintain the microstructure of the fibers, which play a major role for supporting the MSCs growth.

The mechanical properties of biomaterials can greatly influence the attachment, growth, and differentiation behavior of stem cells. Therefore, mechanical tests were performed on SG nanofibers to study the effect of increasing GelMA content on the mechanical behavior.

As it shown in Figure 2I–J, the tensile strength of the nanofibers decreased as more GelMA was incorporated, due to the worse mechanical integrity of GelMA compared to SF. Especially for SG3 and SG5, the mechanical property was significantly decreased due to the high percent of GelMA. SF7 and SF10 showed improved mechanical properties despite of statistically significant difference compared to SF. This demonstrates that SF is important for maintaining the structural and mechanical properties of nanofibers.

2.2. Cytocompatibility of SG electrospun fibrous membrane

Cytocompatibility and cell proliferation were investigated by seeding MSCs on SG nanofibers and preforming a Live/Dead assay (Figure 3). Compared with SF-only fibers, SG nanofibers exhibited significantly improved cell compatibility based on viability results. Although cells remained 80% viable on SF-only scaffolds during a 7-day incubation period, the viability of MSCs seeded on SG scaffolds was significantly elevated to over 90% in the SG10, SG7, SG5 and SG3 groups. The lower cell viability on SF fibers may be due to reduced cell attachment efficiency, resulting from hydrophobic properties and lack of cell binding sites on *Bombyx mori (B. mori)* silk [16]. Cell adhesion can influence cell survival, growth and differentiation through cell machinery involved in the cell cycle [18]. The adhesion of cells to the basement membrane/matrix or to other cells can regulate progression through specific phases of the cell cycle. In particular, it has been reported that the use of polymers that can affect cell adhesion (e.g, polyethylene glycol [19]) can affect cell viability. In our previously reported study of the biocompatible coating of electrodes, we found that the use of polyethylene glycol (PEG), which weakened cell attachment, resulted in a temporary decrease in viability [20]. From this point of view, the fiber hydrophilicity and cell affinity could be improved by incorporating RGD motifs and functional groups in GelMA, which consequently led to higher cell viability. Additionally, cell proliferation results further showed the positive effect of the GelMA content in promoting cell growth in SG groups, which implied that the introduction of GelMA to SF play a crucial role in the growth and proliferation of the MSCs. Fluorescent images of MSCs grown on the nanofibers were recorded to visualize the influence of the nanofibers on the growth state of cells. It was obvious that the cell density on SF and SG15 nanofibers was significantly lower than other groups. Although the cell number in each group increased over time, cells seeded on SG fibers had increased growth compared to SF groups. This further supports the role of GelMA within the SG composited in promoting MSCs growth.

2.3. *q-PCR* analysis

T To evaluate the effect of different compositions of GelMA and SF nanofibers on MSC phenotype, MSCs were cultured on SG3, 5, 7, 10 for 7 days. MSCs cultured with SF-only and GelMA-only nanofibers were used as controls. The tenogenesis-related gene expression levels were evaluated by *q*-PCR. As shown in Figure 4A, changes in the ratio of SF and GelMA result in significant changes in phenotype. Overall, we observed differences in stemness-, growth factor-, tenogenic differentiation-, and extracellular matrix-related gene expression between groups. Genes associated with tenogenesis and extracellular matrix (ECM)-remodeling including *Biglycan, Decorin, Type III collagen (Col III), Matrix metalloproteinase-1 (MMP1), Scleraxis, Fibronectin, MMP2, Alpha-smooth muscle actin (α-sma), Fibromodulin, Col I*, and *Elastin* were down-regulated in MSCs on SF-only

nanofibers. In addition, a downregulation of stemness- and growth factor-related genes such as *Nanog Homeobox (Nanog), VEGF, Fibroblast Growth Factor 2 (FGF2), SRY-Box Transcription Factor 2 (Sox 2)* were also observed. In contrast, MSCs cultured on the GelMA-containing nanofibers showed up-regulated gene expression profiles in tenogenesis/ECM-remodeling (*Biglycan, Decorin, Col III, Scleraxis, Col I, MMP1, Fibromodulin, MMP2*) and stemness/growth factor (*Nanog, Octamer-binding transcription factor 4 [Oct4], VEGF, FGF2*)-related genes compared to the SF group. Interestingly, in the SF7 group, we observed an upregulation of both tenogenesis/ECM-remodeling-related and stemness/growth factor-related genes compared to all other groups [21]. In particular, quantitative analysis revealed that significant up-regulation of *VEGF* (vs SF; 222%, vs GelMA; 147%), *Elastin* (vs SF; 222%, vs GelMA; 150%), *Col I* (vs SF; 275%, vs GelMA; 168%), *Sox 2* (vs SF; 304%, vs GelMA; 294%), *Scleraxis* (vs SF; 211%, vs GelMA; 123%), *Fibronectin* (vs SF; 222%, vs GelMA; 150%), *FGF2* (vs SF; 240%, vs GelMA; 176%), and *Transforming growth factor beta1 (TGF-β1)* (vs SF; 164%, vs GelMA; 410%) (Figure 4B). According to our results, GelMA nanofibers, which are a softer ECM-based material, appear to exhibit favorable properties for tendon regeneration. However, as can be seen from our mechanical testing results, GelMA alone has severe mechanical mismatch with tougher tissues such as tendons and it is difficult to maintain a tension that can withstand the forces of contraction and relaxation during movement. Based on these results, our SG7 composite induces a tendon-friendly MSC phenotype by up-regulating tendon regeneration-related genes while also maintaining improved mechanical properties with SF content.

2.4. Cell attachment and morphology on the SG fibrous membrane

Cell adhesion to the surface of biomaterial is one of the major factors in mediating its biocompatibility and differentiation fate, which can be modulated by the substrate. Therefore, the cell attachment and spreading behavior of MSCs cultured on the SG7 nanofibers were evaluated to further investigate the influence of SG nanofibers on the cell response. MSCs on the nanofibers were stained with phalloidin after 12 h of culture and the morphology of the cells were observed under a fluorescent microscope. As displayed in Figure 5A, MSCs on SG7 nanofibers appeared to stretch and spread into an elongated configuration and cells were more likely to contact each other. While MSCs on SF, GelMA, and tissue culture plate (TCP) groups appeared spherical shape with a few irregular protrusions. We also evaluated the morphology of cells on different substrates with SEM imaging. Cells on SF nanofibers were spherical and poorly adhered to the substrate, while cells on SG7 fibers attached very well with more membrane protrusions interacting with the nanofibers. Cells on GelMA alone substrate adhered smoothly but could not spread very well (Figure 5B). Quantification analysis based on the fluorescent images showed that cells on SG7 and GelMA nanofibers were enlarged; the average single-cell area was significantly larger than cells on SF and TCP groups. It was also noteworthy that even though cells grown on SG7 and GelMA nanofibers could both spread very well and exhibit a larger cell area, the MSCs in the GelMA group showed a lower aspect ratio and higher circularity compared to the SG7 group. This is because the combination of soft GelMA and better mechanical properties of SG7 fibers could provide physical guidance for the growth and spread of MSCs and consequently promoted elongation and stretching. Statistics of cell attachment ratios displayed in Figure S3 showed that 8 hours after seeding more than 80% of cells were

attached on SG7, GelMA and TCP group but the SF group exhibited low cell attachment percentage (~60 %). Combination of a fibrous scaffold to provide mechanical resilience, a hydrogel system to carry the cells has been demonstrated to be a possible integrated solution to accommodate for the variations in the cells used for tendon repair [22]. While in our study, GelMA was directly co-electrospun with SF to simultaneously provide ECM-like local environment for cell attachment, spread, and keep the porous structure of fibrous sheet for cell infiltration. From the results, we can confirm that GelMA component in SG7 nanofibers provides suitable adhesion sites via intrinsic adhesion peptides that are critical for MSC growth and the spreading processes. In combination with improved stiffness and microstructure of SG7, MSCs could attach and spread well on the substrate, express tendon- and growth factor-related genes.

2.5. VEGF secretion ability and *in vitro* wound healing analysis of SG fibrous scaffold

It has been shown that different substrates and material surface properties have great influence on cell morphology and, therefore, a profound influence on cytokine expression. VEGF is one of the most important growth factors for the growth and proliferation of cells during the wound healing process. Moreover, severe cartilage, tendon, and ligament injuries usually have low intrinsic healing capacity because of the lack of vascularization and poor blood supply [23]. Secreted VEGF can initiate the formation of vascular networks, which is very critical for promoting and supporting the newly formed tissue during the early proliferation phase of *in vivo* tendon healing [24]. Therefore, the VEGF secretion levels of the MSCs grown on different nanofibers were investigated and compared to determine the influence of the material composition on the cell functions (Figure 6A). As shown in Figure 6B, MSCs cultured on SF, SG7 and GelMA nanofibers exhibited significantly higher secretion levels of VEGF compared to those cultured on TCP. The SG7 group demonstrated the highest level of VEGF secretion, especially between the 4th and 7th day of culture. The cumulative VEGF secretion amount at different time points displayed in Figure 6C further proved that MSCs cultured on SG7 fibers have significant increases in VEGF secretion compared with other groups. This observation correlates with our quantitative polymerase chain reaction (qPCR) results and implies that the positive interactions between SG7 fibers and MSCs can modulate the growth factor secretion. It has been demonstrated that VEGF is associated with the expression of Col I and other extracellular molecules [24a]. Therefore, we evaluated the influence of MSC-conditioned media on tenocyte proliferation and migration using an *in vitro* tendon wound healing scratch assay model. The viability test using Cell Counting Kit-8 (CCK-8) results and fluorescent images of tenocytes incubated in MSC-conditioned medium obtained at Day 7 displayed in Figure S4 implied that conditioned medium of MSCs cultured on SG7 nanofibers could apparently promote the proliferation of tenocytes compared to other groups. Moreover, for the *in vitro* wound healing evaluation, scratched tenocyte monolayers were imaged initially and at different time points to evaluate the cell migration distance and wound closure rate. As shown in Figure 6D, MSCs cultured on SG7 using MSC-conditioned medium obtained at Day 7 could significantly enhance the tenocytes migration and consequently promote the closure of the wound. Wound closure rates further confirmed that the effect on tenocytes migration was greatest in SG7 group compared with other groups (Figure 6E). Therefore, the SG7 positively influences the secretion of VEGF, which plays a crucial role in wound healing and could significantly

promote tendon tissue regeneration by influencing the cell behavior of tenocytes. As it reported in previous studies, the biological effect of most reported fibrous scaffold usually greatly relied on the incorporation of growth factors. For instance, Bone Morphogenic Protein-13 (BMP-13) has been introduced to a SF-collagen hybrid scaffold to promote the tenocytes migration [25]. While the SG7 fibers without any additional biomolecules (growth factors) could significantly promote the growth factor secretion to support the migration of tenocytes, indicating the appropriate incorporation of GelMA and rational design of SG fibers endowed the fibrous sheet with remarkably positive biological performance.

2.6. *In vivo* biocompatibility and degradation analysis

Before evaluating the therapeutic efficacy of electrospun nanofibers, we first examined the biocompatibility and biodegradability of SG7, SF and GelMA nanofibers for 4 weeks (Figure S5). Nanofibers were subcutaneously implanted into the back of rats. As shown in Figure S5A, GelMA nanofibers degraded rapidly over time, while SF groups barely degraded. On the other hand, the SG7 group degraded slower than GelMA, but the degradation rate was significantly faster than that of SF. No significant inflammation was observed around the implanted nanofibers in all transplanted groups. As the degradation proceeded, fibrous tissue accumulation was observed around the nanofibers in all groups, especially in the SF group with slow degradation. Quantitative analysis showed that 2 weeks after transplantation, GelMA was degraded by an average of 75.3% normalized to SF, while SG7 was only degraded by an average of 42.5% (Figure S5B). Therefore, these results indicate that SG7 remains in its shape for an appropriate period (>2 weeks) during the several weeks to months process of tendon regeneration, making it a suitable scaffold for tendon therapy.

2.7. *In vivo* tendon regeneration efficacy

Finally, we investigated the therapeutic efficacy of SG7 using a rat Achilles tendon injury model (Figure 7A). All nanofibers with MSCs adhered well to tendon tissue after implantation, making the SG fibers more practical for clinical application compared with conventional scaffolds which usually require secure process for fixation [22d, 26]. 2 and 4 weeks after surgery, in the injury-only group, the damaged area was thicker than normal (Figure 7B). Electrospun sheets were located on the site of injury and no tissue changes (discoloration, increased tendon thickness) were observed [27]. Similar to the subcutaneous implantation results, all material in the GelMA+MSCs group degraded at 4 weeks and were not observed. With microscopic gross evaluation following hematoxylin and eosin (HE) staining, the sectional tendon thickness increased more in the injury group compared to the other groups. In addition, damaged and regenerated tendon structures were still observed in all groups at 2 weeks. However, in the MSC-loaded groups (MSC injection, GelMA+MSCs, SF-only+MSCs, SG7+MSCs), tendon injury sites were relatively reduced compared to the injury group (Figure 7C). In Masson’s trichrome (MT) staining, the damaged tendon fibers showed weak MT positives (low collagen deposition) as shown by the dotted red line in Figure 7C. However, the SG7 group had fewer weak MT positive areas than the other groups, and the newly formed tendon fibers were also relatively densely packed and well-organized. Even after 4 weeks, loosely unorganized structures were still observed in the injury group. MSC-loaded groups (MSC injection, GelMA+MSCs,

SF+MSCs, SG7+MSCs) showed relatively well-aligned, densely packed, and regenerated tendons compared to the injury group. In the MT staining, the control group showed MT negative (red) muscle components at both weeks 2 and 4. Interestingly, the SG7 group also showed an MT negative area similar to that of the control group in the tendon at 4 weeks. Quantitative analysis of MT staining also showed that significant higher positive intensity in the SG7+MSCs group than any other injured groups (Figure 7D). Consistent with *in vitro* tenogenesis/ECM-remodeling-related gene expression analysis results, this result demonstrated that the MSC-loaded SG7 accelerated the regeneration of damaged tendons and remodeling into muscle components.

Then, we performed immunofluorescence analysis of tendon proteins including Col I, Col III, Pro-collagen I (ProCol I), and tenomodulin (TNMD) to analyze the extent of regeneration following injury. The regenerative process of the tendon involves various cellular and molecular changes throughout three phases, inflammatory, reparative, and remodeling [21]. In general, 90% of the tendon protein content is collagen, of which Col I accounts for almost 95%. Col III and ProCol I are the main matrix protein formed by the fibroblasts recruited in the earlier stage of regeneration. TNMD is primarily a tendon-specific marker that is involved in the regulation of tenocyte proliferation. The remodeling phase begins with the replacement of Col III by Col I [2a, 27]. As shown in Figure 8, the expression of Col I in the injury-only group was markedly decreased, whereas the expression of Col III was increased at 4 weeks. The expression levels of Col I and Col III protein in the SG7+MSCs group were significantly higher than other groups at 2 weeks. In particular, compared to the groups of MSC injection, GelMA+MSCs, and SF+MSCs, SG7+MSCs group showed that the Col I positive fibers were aligned in one orientation. Moreover, the fluorescence signal of Col III was barely detected at 4 weeks in the SG7 group. The production of mature tenocytes usually requires a tendon-specific matrix with a higher level of Col I and a lower level of Col III [28]. These results showed that the SG7+MSCs group was faster in regeneration and remodeling to the normal tendon protein expression than any other groups.

Moreover, the expression of ProCol I and TNMD were also significantly upregulated in the SG7+MSCs group at 2 weeks, indicating the enhanced tendon-related stem cell and fibroblast activities (Figure S6 & 7). Similar to Col III, the expression levels of ProCol I and TNMD of the SG7 group were decreasing at 4 weeks. Combined with the analysis of Col I and Col III expression, these results indicate the gradual integration of newly formed tendon tissues (weak Col I, strong Col III, TEND, ProCol I) with the regenerated/normal tissue (strong Col I, weak Col III, TEND, ProCol I). Taken together, our results suggest that MSC-loaded SG7 can improve the growth and maturation of MSCs that stimulate tendon regeneration *in vivo*.

3. Conclusion

In this study, GelMA was introduced to SF to produce a nanofibrous scaffold for tendon tissue repair. The electrospun sheet with a suitable structure that supported the attachment and growth of MSCs was achieved when the weight ratio of SF and GelMA was 7:1 (SG7). The obtained SG7 sheets with high biocompatibility and good mechanical properties

could efficiently promote the proliferation of MSCs and provide a good microenvironment, which greatly promoted the tendon tissue reconstruction. The marker genes associated with tendon differentiation confirmed that SG7 could induce the tenogenic differentiation of MSCs. Further study showed that SG7 could positive influence MSC attachment, spreading, and subsequent VEGF secretion. *In vitro* and *in vivo* tendon repair analysis indicated that the SG7 scaffold could effectively fix MSCs at injured sites, provide favorable microenvironment for MSCs growth, and induce the tendon regeneration-related cytokines secretion as well as tenogenic differentiation of MSCs simultaneously, which consequently greatly promote the healing of tendon injuries and this combination strategy could be a promising method in tendon tissue regeneration applications.

4. Experimental Section

Preparation of silk fibroin:

A solution of silk fibroin was prepared from *Bombyx mori* silkworm cocoon (Uljin farm, South Korea). To get the silk fibroin by removing Sericin, a degumming process was conducted. The cocoons were boiled for 30 min in 0.01 M of sodium oleate (O7501, Merck, USA) and 0.2M of sodium carbonate anhydrous (451614, Merck, USA) aqueous solution. After drying process, the silk fibroin was dissolved for 30 min in a 9.3M lithium bromide (213225, Merck, USA) solution at 60 °C and dialyzed in deionized (DI) water for 48 hours.

Preparation of GelMA:

Porcine gelatin (G2500, Merck, USA) was dissolved for 1 hours at 10% (w/v) in 100 mL Dulbecco's phosphate-buffered saline (PBS) at 50 °C. Subsequently, 8 mL methacrylic anhydride (276685, Merck, USA) was dissolved in the gelatin-PBS solution and stirred for 2 hours at 50 °C for methacrylation. In order to stop the reaction, 100 mL PBS was added at 50 °C. Then, the solution was dialyzed at 40 °C for 7 days using dialysis membranes (Fisher Scientific, M_w cut off: 12–14 kDa) to remove the impurities. The purified solution was filtrated by a vacuum filtration cup (Millipore Sigma, pore size : 0.22 μm). This solution was frozen at −80 °C freezer and then lyophilized.

Fabrication of electrospun sheet:

A 10% SF solution was prepared in formic acid and stirred slowly overnight. A 10% GelMA solution was prepared in formic acid and stirred slowly for 2 hours. Then we mixed SF and GelMA solution with different ratio (SF:GelMA = 15:1, 10:1, 7:1, 5:1 and 3:1 (w/w)). The fibers were electrospun under a voltage of 22 kV. The infuse rate of solution was 0.5 ml/h and the distance between the needle and the 100 cm^2 collector (aluminum foil) was 15 cm. The obtained fibers were denoted as SG15, SG10, SG7, SG5 and SG3 according to the rations between GelMA and SF. For the electrospinning of GelMA-only fibers, GelMA was first dissolved in formic acid with a concentration of 10% (w/v). The parameters for electrospinning were 22 kV voltage, 0.2 mL/h feed rate and 15 cm distance from needle to collector plate. For the crystallization of SF and crosslinking of GelMA, the photoinitiator 2-hydroxy-4'-(2-hydroxyethoxy)-2-methylpropiophenone (Irgacure 2959, Sigma Aldrich) was dissolved in 99.9% methanol in the absence of light. Then, the uncrosslinked fiber sheets were immersed in the solution and irradiated by 365 nm UV light (200 mW/cm^2) for

3 min. Then the prepared samples were immersed in DI water for 12 h to remove excess photoinitiator.

Mechanical property test of SG nanofibers:

Mechanical property of all groups of electrospun sheets were measured by a universal testing machine (Instron 5943, MA, USA). The samples of electrospun sheet were cut into a rectangular shape (2 cm × 1 cm). A tensile test was performed at 0.5 mm/min tensile strain until failure was observed, and the tensile force with respect to displacement was recorded.

MSCs culturing and cell viability test:

Human bone marrow-derived stem cells purchased from ATCC were employed in all the cell experiments in this study. To study the cell compatibility of the electrospun sheets, the obtained fiber membranes were sterilized by exposure to UV irradiation for 30 min. Then, MSCs were seeded on the electrospun samples with a density of 5000 cells/well and cultured in Dulbecco's Modified Eagle Medium (DMEM, low glucose) containing 10% fetal bovine serum (FBS) at 37 ºC under a 5% CO_2 humidified atmosphere. After culturing for 1, 4, or 7 days, the medium was removed, and the cell-laden electrospun sheets were washed with PBS twice. Following, a Live/Dead Viability/Cytotoxicity Kit (Thermo Fisher, USA) was performed following the manufacturer's instructions to assess the cell viability. The survival/death ratio was analyzed by counting the number of living and dead cells in 5 or more non-overlapping regions of 3 or more samples (Green/Red ratio). Cell proliferation was analyzed by dividing the live cell counting of each day and sample by the live cell counting of Day 1 TCP. Total cell number and fluorescence value were quantified with NIH Image J analysis software.

Analysis of cell attachment and morphology:

Cell attachment was investigated by seeding the cells on the SG7 fibers with a density of 8000 cells/well in 96 well plate. After culturing for 6 h, the cell medium was removed, and the wells were washed 3 times with PBS. After washing, cells were fixed with 3.7% paraformaldehyde for 20 min, and the cell nucleus was stained by 4',6-diamidino-2-phenylindole (DAPI) for 20 min. Then the number of the attached cells were counted. GelMA-only and SF-only sheets were used as control. For observing the cell attachment behavior, cells were seeded on the SG7 with a density of 5000 cells/well in 96 well plates. After culturing for 12 h, the medium was removed and the cells on SG7 were washed with PBS 3 times. Then, cells were fixed with 3.7% paraformaldehyde for 20 min. The fixed cells were washed with PBS for 3 times and permeabilized with 0.1% Triton X-100 for 20 min, followed by an additional two PBS washes. Then, cells were blocked in 1% albumin bovine serum albumin (BSA) solution for 40 min and stained with phalloidin-FITC (Sigma) at room temperature in a dark environment for 30 min. After 3 additional PBS washes, the stained cells were observed under the fluorescent microscope (Zeiss). At least five non-overlapping images were taken for each sample and the cell area, aspect ratio and circularity of singles cells were quantified with Image-J software.

SEM images of cells cultured on the SG7 sheets were also recorded to investigate the influence of the nanofibers on the MSC attachment. SG7 sheets were placed in a 48 well

plate and MSCs were seeded on the sheets with a density of 5000 cells/well. After culturing for 1 day, the medium was taken out and the cells were washed with PBS for 2 times. Then the cells were fixed with 3.7% glutaraldehyde for 12 h at 4 ºC. After washing with PBS 2 times, the cells were further fixed by 1% osmium tetroxide solutions for 1 h. After that, the samples were washed with PBS for 2 times and dehydrated following an ethanol series dehydration process. Finally, the samples were taken for SEM imaging after completely drying at room temperature.

Enzyme-linked immunosorbent assay (ELISA) analysis for measurement of VEGF secretion:

Human VEGF secretion was evaluated to investigate the influence of the fibers on the secretion of paracrine factors by seeded MSCs. MSCs were seeded on the SG7 with a density of 25000 cells/cm^2 and cultured for 10 days. The medium was collected on the 4th, 7th and 10th day of culture and evaluated with a Human VEGF sandwich assay ELISA (Sigma-Aldrich) following the manufacturer's instructions. Specifically, 100 μl of standard or sample was added to the plate with capture antibody and incubated at room temperature for 2.5 h. Then, the standard or sample was removed and washed with wash buffer for 4 times. 100 μl detection antibody was provided to the wells and incubated for 1 h. Subsequently, 100 μl of streptavidin was provided and incubated for 45 min after washing. Each well was washed again and 100 μl of substrate was provided and further incubated for 30 min. Finally, 50 μl of stop solution was added and the samples were directly measured by the plate reader (BIOTEK Fluorescent plate reader, Synergy HTX multimode reader) at the wavelength of 450 nm. TCP, SF-only, and GelMA-only groups were used as controls.

Cell migration test:

To investigate the influence of paracrine factors secreted from MSCs cultured on electrospun sheets on the migration of tenocytes, MSC conditioned medium was collected and applied to tenocytes. MSCs were seeded on the SG7 with a density of 5000 cells/cm^2 and cultured for 10 days. The conditioned medium was collected at the 4th, 7th, and 10th day of culture. The collected conditioned medium was mixed together and stored at −20ºC for further use. The conditioned medium of MSCs cultured on SF, GelMA, and TCP were used as control. Human Tenocytes (Zen Bio) were seeded in 12 well plate with a density of 10^5 cells/well and cultured at 37 °C and 5% CO_2 in high glucose DMEM (Gibco) along with 1% penicillin/streptomycin and 10% FBS. After the cells were confluent, the cell medium was removed and a uniform ~0.5 mm width scratch was created by scraping the confluent cell layers with a sterile pipette. Then, the cells were cultured in MSCs conditioned medium or fresh DMEM with 10% FBS. The images of the scratched wound were taken at predetermined time points to evaluate the migration of the cells.

qPCR analysis:

MSCs were seeded on SG3, SG5, SG7 and SG10 with a concentration of 10^6 cells per 100 mm culture dish and cultured for 7 days. SF-only and GelMA-only were used as control. Total RNA was extracted using a RNeasy plus mini kit (Qiagen, CA, USA). The QuantiTect Reverse Transcription Kit was used to transcribe total RNA into the cDNA. The expression levels of target genes were evaluated by real-time PCR using the QuantStudio 3

(ThermoFisher Scientific). Reaction conditions are as follow: initial denaturation, 5 min at 95 °C; recurring denaturation, 5 s at 95 °C, and amplification, 10 s at 60 °C, for 45 cycles. The relative expression level of all the mRNA was calculated and normalized by using the $2^{-\Delta\Delta Ct}$ method, with glycer-aldehyde 3-phosphate dehydrogenase (GAPDH) and β-actin as reference genes. The primer sequences of the targeted genes were displayed in Table S1.

In vivo biocompatibility and biodegradability investigation:

All animal experiments were approved and conducted in compliance with the relative guidelines of the UCLA Animal Research Committee (#2018–004-01E). Twenty-four, eight-week-old male rats (Sprague-Dawley rats, 250–300 g) were obtained from Charles River Laboratories (Sacramento, CA, USA). Animals were randomly divided into 3 groups: SG7, SF, GelMA (n=4 per each group and each timepoint [2, 4 weeks]). SG7, SF, and GelMA groups with a size of 1 cm × 0.5 cm were subcutaneously implanted (4 samples per each animal) in the back of rats under inhalation anesthesia (1.5% isoflurane in 100% O_2). In each time point (14 and 28 days), four animals per group (SG7, SF, GelMA) were sacrificed and the skin tissue with the implanted samples were collected for biocompatibility and biodegradability evaluation. The skin samples were fixed in 10% neutral buffered formalin (NBF) for histological analysis. All samples were trimmed in the same way, cutting the center of the skin containing the sample into a sagittal cross section to provide the maximum area of the sample area. The weight of different samples was recorded at different time points and the weight ratio of remaining nanofibers to the samples were calculated to analyze the degradability.

In vivo rat Achilles tendon repair model:

The therapeutic efficacy of the SG nanofibers was investigated *in vivo* using an Achilles tendon injury model. Forty-eight, eight-week-old male Sprague Dawley (SD) rats (average weight: 250–300 g) were purchased and housed in an approved animal facility (UCLA animal protocol: #2018–004-01E). Surgical procedures were conducted under inhalation anesthesia (1.5% isoflurane in 100% O_2). To expose the Achilles tendon, a longitudinal skin incision (1–2 cm) was made parallel to the tendon fibers. After blunt separation of the surrounding tissue to release the tendon, a crush injury was applied to the mid-central area of the tendon tissues for 5 minutes using a 100 g vascular clip (Fine Science Tools, Foster City, CA, USA). Animals were randomly divided into 6 groups: SG7, SF, GelMA, MSC Injection, injury, and uninjured control (n=4 per each group, each timepoint [2, 4 weeks]). For the experimental groups, 5×10^4 cells/cm^2 of MSCs were seeded on sterilized SG7, SF, and GelMA sheets, and, after culturing for 2 days, the scaffolds were applied to the wound area. For the MSCs injection group, the same amount of MSCs were directly injected into the wound sites. The wound was then carefully washed with the sterilized saline and the skin was closed with 4–0 non-absorbable sutures.

Histology and immunofluorescent analysis:

SD rats were sacrificed at 2 weeks and 4 weeks after surgery. The collected tendon samples were fixed in 10% NBF, dehydrated in ethanol, and embedded in paraffin. Slides with 4 μm sections were obtained and used for hematoxylin and eosin (H&E) and Masson's trichrome (Masson) staining. For the quantitative analysis of Masson staining positive area in the

lesion, at least three 1x magnification images of the slides were collected using an optical inverted microscope (Amscope, USA). The intensity of Masson positive area in the lesion was measured on at least five microscopic areas of each sample using Image-J software. The relative intensity was obtained by comparing measured intensity with the Control group.

For immunofluorescence analysis, the sections were immersed in citrate-buffered antigen retrieval buffer and then subjected to pressured antigen retrieval for 30 minutes to liberate antigens. The slides were then permeabilized in PBST (PBS+0.3% Triton) for 20 min and blocked with 5% goat serum albumin for 30 min at room temperature. After that, the slides were incubated primary antibodies 4 °C overnight. The primary antibodies used in this study are following: rabbit Col I antibody (1:100, Abcam) and mouse Col III antibody (1:100; Abcam), rabbit TNMD antibody (1:100, Abcam), rabbit ProCol I antibody (1:100, Abcam). Anti-rabbit Alexa 555 conjugated secondary antibody (1:1000, Abcam) and Anti-mouse Alexa 488 conjugated secondary antibody (1:1000) were used as secondary antibodies. To visualize nuclei, sections were counterstained with DAPI (Fisher Scientific, USA) for 5 min. At least three 400x magnification fluorescence images of the slides were collected on a fluorescence microscope (Zeiss). For the quantitative analysis, the fluorescence intensity was measured for each fluorescence wavelength (green, red) in each sample using Image-J software. The relative intensity was obtained by comparing each measured fluorescence intensity with 2 weeks Control group.

Statistical analysis:

All data were collected in at least triplicate, and the mean ± standard deviation (SD) was measured with GraphPad Prism software (version 9.3.1) and OriginPro (version 8.5.0). Data for experiments were analyzed using one-way analysis of variance (ANOVA), followed by Bonferroni post-hoc comparisons test for multiple comparisons. A p value ≤ 0.05 between experimental groups were considered statistically significant.

Supplementary Material

Refer to Web version on PubMed Central for supplementary material.

Acknowledgements

Y. Xue and H-J Kim contributed equally to this work. The authors also acknowledge funding from the National Institutes of Health (EB021857, EB022403 and R01EB021857) and from National Research Foundation of Korea (NRF) grant funded by the Korea government (MSIT) (2021R1F1A105502211). Y. Xue acknowledge the support from China Scholarship Council.

References

[1]. Eekhoff JD, Iannucci LE, Lake SP, Nat. Biomed. Eng 2021, DOI: 10.1038/s41551-021-00724-x.

[2]. a)Nourissat G, Berenbaum F, Duprez D, Nat. Rev. Rheumatol 2015, 11, 223; [PubMed: 25734975] b)No YJ, Castilho M, Ramaswamy Y, Zreiqat H, Adv. Mater 2020, 32, 1904511.

[3]. Gracey E, Burssens A, Cambre I, Schett G, Lories R, McInnes IB, Asahara H, Elewaut D, Nat. Rev. Rheumatol 2020, 16, 193. [PubMed: 32080619]

[4]. a)Fernandez-Yague MA, Trotier A, Demir S, Abbah SA, Larranaga A, Thirumaran A, Stapleton A, Tofail SAM, Palma M, Kilcoyne M, Pandit A, Biggs MJ, Adv. Mater 2021, 33, 2008788;b)Lomas AJ, Ryan CNM, Sorushanova A, Shologu N, Sideri AI, Tsioli V, Fthenakis

GC, Tzora A, Skoufos I, Quinlan LR, O'Laighin G, Mullen AM, Kelly JL, Kearns S, Biggs M, Pandit A, Zeugolis DI, Adv. Drug. Deliver. Rev 2015, 84, 257;c)Howell K, Chien C, Bell R, Laudier D, Tufa SF, Keene DR, Andarawis-Puri N, Huang AH, Sci. Rep 2017, 7, 45238. [PubMed: 28332620]

[5]. a)Li W, Midgley AC, Bai Y, Zhu M, Hong C, Wang L, Wang Y, Wang H, Kong D, Biomaterials 2019, 224, 119488;b)Nakajima T, Nakahata A, Yamada N, Yoshizawa K, Kato TM, Iwasaki M, Zhao C, Kuroki H, Ikeya M, Nat. Commun 2021, 12, 5012; [PubMed: 34408142] c)Stauber T, Wolleb M, Duss A, Jaeger PK, Heggli I, Hussien AA, Blache U, Snedeker JG, Adv. Healtc. Mater 2021, 10, 2100741.

[6]. a)Rinoldi C, Kijenska-Gawronska E, Khademhosseini A, Tamayol A, Swieszkowski W, Adv. Healthc. Mater, 2021, 10, 2001305;b)Jiang X, Wu S, Kuss M, Kong Y, Shi W, Streubel PN, Li T, Duan B, Bioact. Mater 2020, 5, 636; [PubMed: 32405578] c)Wu S, Liu J, Qi Y, Cai J, Zhao J, Duan B, Chen S, Mater. Sci. Eng., C 2021, 126, 112181.

[7]. Kim SE, Kim JG, Park K, Tissue Eng. Regener. Med 2019, 16, 467.

[8]. a)Costa-Almeida R, Calejo I, Gomes ME, Int. J. Mol. Sci 2019, 20, 3002; [PubMed: 31248196] b)Yea JH, Bae TS, Kim BJ, Cho YW, Jo CH, Acta Biomater. 2020, 114, 104; [PubMed: 32682057] c)Abbah SA, Spanoudes K, O'Brien T, Pandit A, Zeugolis DI, Stem Cell Res. Ther 2014, 5, 38. [PubMed: 25157898]

[9]. a)Shojaee A, Parham A, Stem Cell Res. Ther 2019, 10, 181; [PubMed: 31215490] b)Wang X, Rivera-Bolanos N, Jiang B, Ameer GA, Adv. Funct. Mater 2019, 29, 1809009;c)Wan X, Liu Z, Li L, Adv. Funct. Mater 2021, 31, 2010626;d)Hilfiker A, Kasper C, Hass R, Haverich A, langenbecks arch. surg 2011, 396, 489. [PubMed: 21373941]

[10]. a)Migliorini F, Tingart M, Maffulli N, Expert Opin. Biol. Ther 2020, 20, 1373; [PubMed: 32574078] b)Walden G, Liao X, Donell S, Raxworthy MJ, Riley GP, Saeed A, Tissue Eng., Part B 2017, 23, 44;c)Hoffmann A, Gross G, Int. Orthop 2007, 31, 791; [PubMed: 17634943] d)Chen S, Wang J, Chen Y, Mo X, Fan C, Mater. Sci. Eng. C 2021, 119, 111506.

[11]. a)Liu Q, Zhu Y, Zhu W, Zhang G, Yang YP, Zhao C, Biomaterials 2021, 277, 121083;b)Rinoldi C, Costantini M, Kijenska-Gawronska E, Testa S, Fornetti E, Heljak M, Cwiklinska M, Buda R, Baldi J, Cannata S, Guzowski J, Gargioli C, Khademhosseini A, Swieszkowski W, Adv. Healthc. Mater 2019, 8, 1801218;c)Yta B, Cca C, Fei L, Sxab D, Jin QA, Mla B, Zan L, Xl A, Qiang S, Sla B, Biomaterials 2020, 241, 119837.

[12]. Lu K, Chen X, Tang H, Zhou M, He G, Lu Z, Tang K, Stem Cells Int. 2020, 2020, 8857380.

[13]. Tsai SL, Nodl MT, Galloway JL, Dev. Dyn 2021, 250, 393. [PubMed: 33169466]

[14]. Liu LD, Hindieh J, Leong DJ, Sun HB, J. Orthop. Translat 2017, 9, 69. [PubMed: 29662801]

[15]. a)Wu R, Li H, Yang Y, Zheng Q, Li S, Chen Y, ACS Appl. Bio Mater 2021, 4, 6630;b)Farokhi M, Mottaghitalab F, Fatahi Y, Saeb MR, Zarrintaj P, Kundu SC, Khademhosseini A, Eur. Polym. J 2019, 115, 251.

[16]. Maghdouri-White Y, Petrova S, Sori N, Polk S, Wriggers H, Ogle R, Ogle R, Francis M, Biomed. Phys. Eng. Express 2018, 4, 025013.

[17]. Yue K, Trujillo-de Santiago G, Alvarez MM, Tamayol A, Annabi N, Khademhosseini A, Biomaterials 2015, 73, 254. [PubMed: 26414409]

[18]. a)Gumbiner BM, Cell 1996, 84, 345; [PubMed: 8608588] b)Pugacheva EN, Roegiers F, Golemis EA, Current opinion in cell biology 2006, 18, 507; [PubMed: 16919436] c)Ruijtenberg S, van den Heuvel S, Cell cycle 2016, 15, 196. [PubMed: 26825227]

[19]. Kord Forooshani P, Lee BP, J Polym Sci A Polym Chem 2017, 55, 9. [PubMed: 27917020]

[20]. Lee YJ, Kim HJ, Kang JY, Do SH, Lee SH, Advanced healthcare materials 2017, 6, 1601022.

[21]. Docheva D, Muller SA, Majewski M, Evans CH, Adv. Drug. Deliver. Rev 2015, 84, 222.

[22]. a)Jiang XP, Wu SH, Kuss M, Kong YF, Shi W, Streubel PN, Li TS, Duan B, Bioact. Mater 2020, 5, 636; [PubMed: 32405578] b)Zhao TF, Qi YY, Xiao SN, Ran JS, Wang JK, Ghamor-Amegavi EP, Zhou XP, Li HYZ, He T, Gou ZR, Chen QX, Xu K, J. Mater. Chem. B 2019, 7, 2201; [PubMed: 32073579] c)Leong DJ, Sun HB, Ann. N. Y. Acad. Sci 2016, 1383, 88; [PubMed: 27706825] d)Li W, Midgley AC, Bai Y, Zhu M, Hong C, Zhu W, Wang L, Wang Y, Wang H, Kong D, Biomaterials 2019, 224, 119488.

[23]. Ding YP, Li W, Zhang F, Liu ZH, Ezazi NZ, Liu DF, Santos HA, Adv. Funct. Mater 2019, 29, 1802852.

[24]. a)Tang JB, Wu YF, Cao Y, Chen CH, Zhou YL, Avanessian B, Shimada M, Wang XT, Liu PY, Sci. Rep 2016, 6, 20643; [PubMed: 26865366] b)Titan AL, Foster DS, Chang J, Longaker MT, Plast. Reconstr. Surg 2019, 144, 639e.

[25]. Yas M-W, Stella P, Nardos S, Seth P, Hilary W, Rebecca O, Roy O, Michael F, Biomed. Phys. Eng. Express 2018, 4, 025013.

[26]. Manning CN, Schwartz AG, Liu W, Xie J, Havlioglu N, Sakiyama-Elbert SE, Silva MJ, Xia Y, Gelberman RH, Thomopoulos S, Acta Biomater. 2013, 9, 6905. [PubMed: 23416576]

[27]. Rodrigues MT, Reis RL, Gomes ME, Tissue Eng J. Regener. Med 2013, 7, 673.

[28]. Parmar K, Orthop. Traumatol 2018, 32, 241.

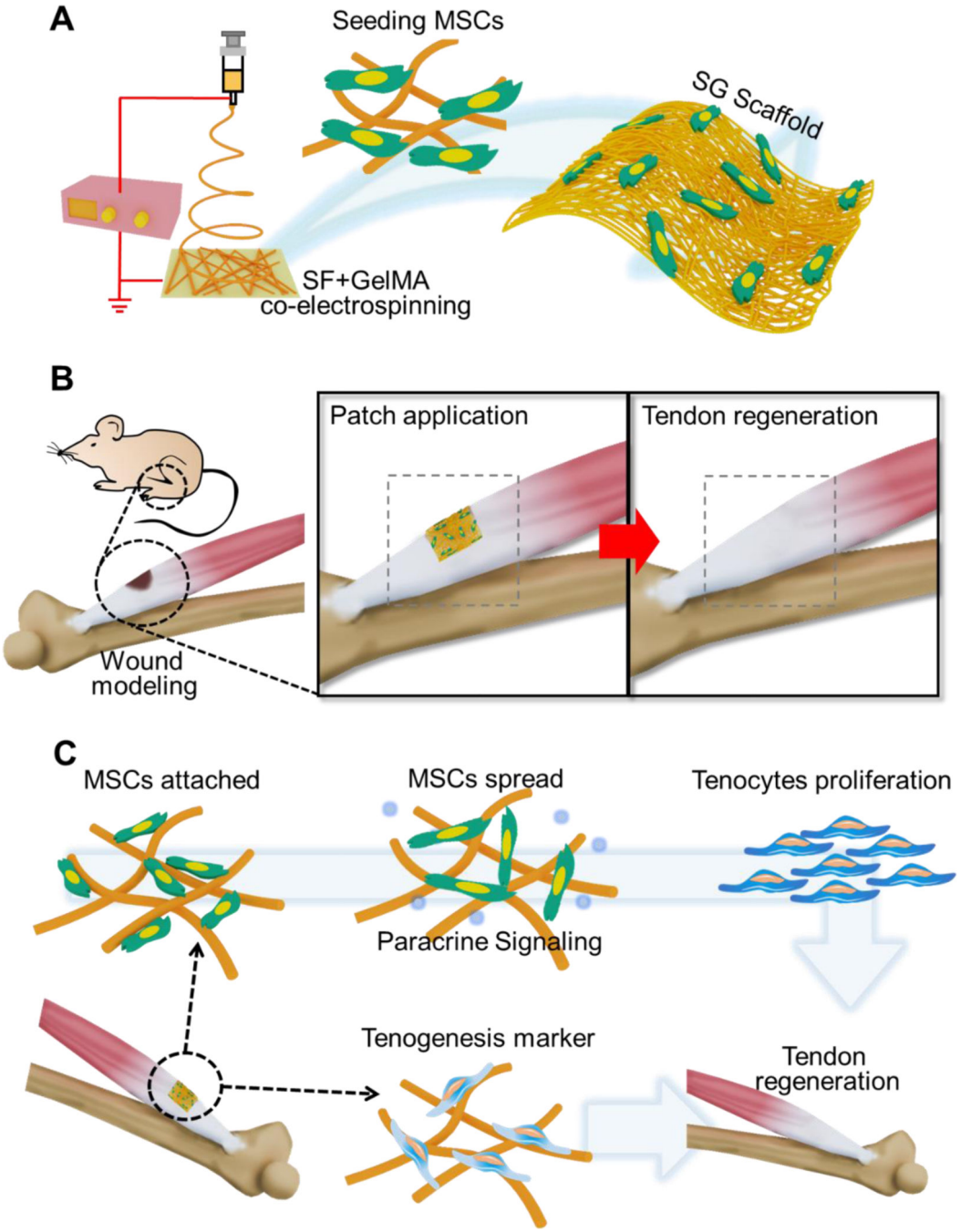

Figure 1.

Diagram of SG fibrous scaffold preparation and application. (A) Schematic of the fabrication of SG fibrous scaffold. (B) The application of SG fibrous scaffold for tendon tissue regeneration. (C) The mechanisms of the SG scaffold during in situ tendon tissue reconstruction.

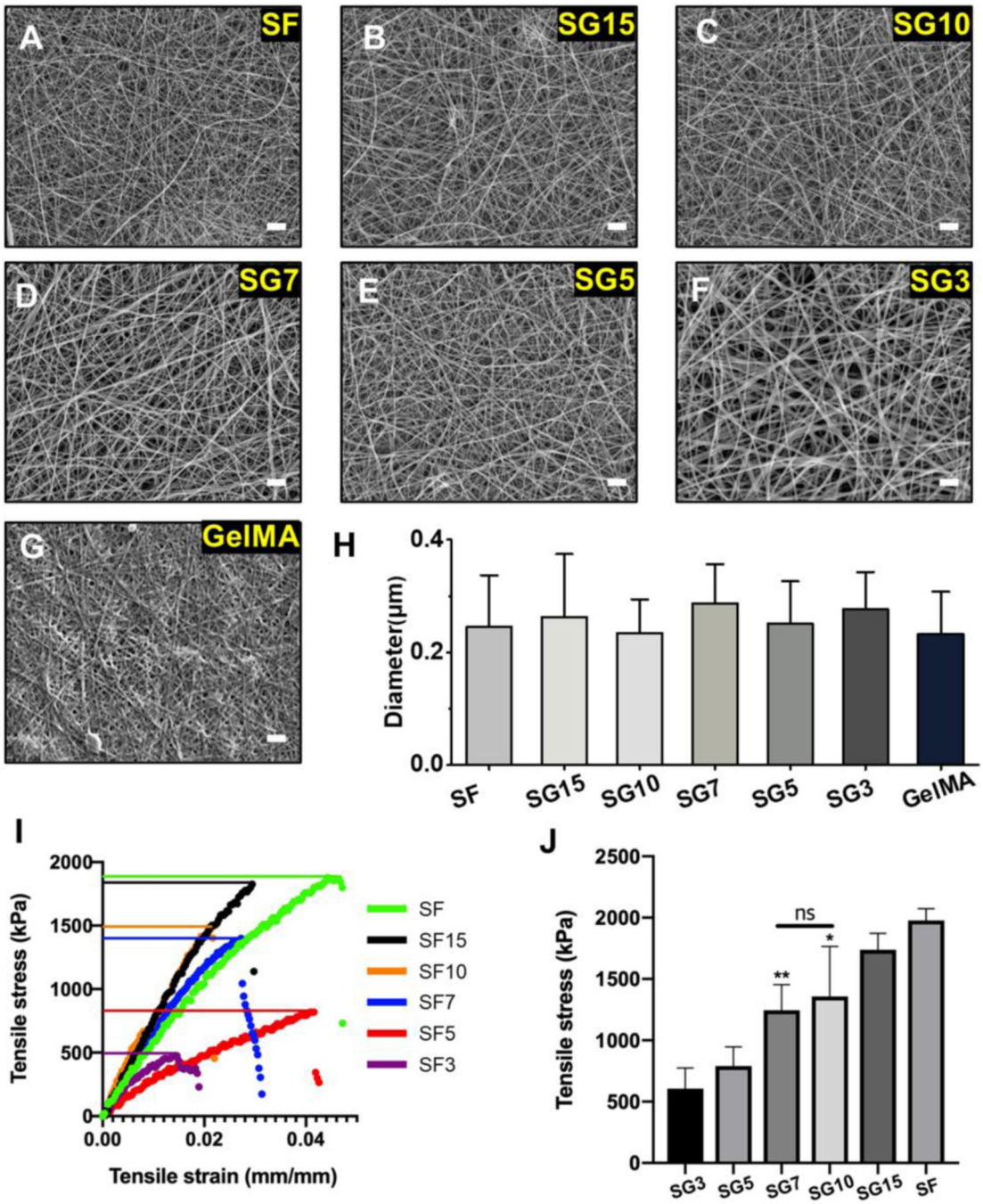

Figure 2.

Morphology characterization and mechanical properties of the SG nanofibers. (A-G) SEM images of SF, SG and GelMA nanofibers. (Scale bar = 2 μm) (H) Quantification of the diameter of SF, SG and GelMA nanofibers based on the SEM images. (I) Representative stress-strain curves of SF and SG7 nanofibers. (J) Breaking strength of SF and SG7 nanofibers. Results are expressed as mean SD of three replicates of experiments. ANOVA (n = 3, $*p < 0.05$, $**p < 0.01$ compared with SF-only group)

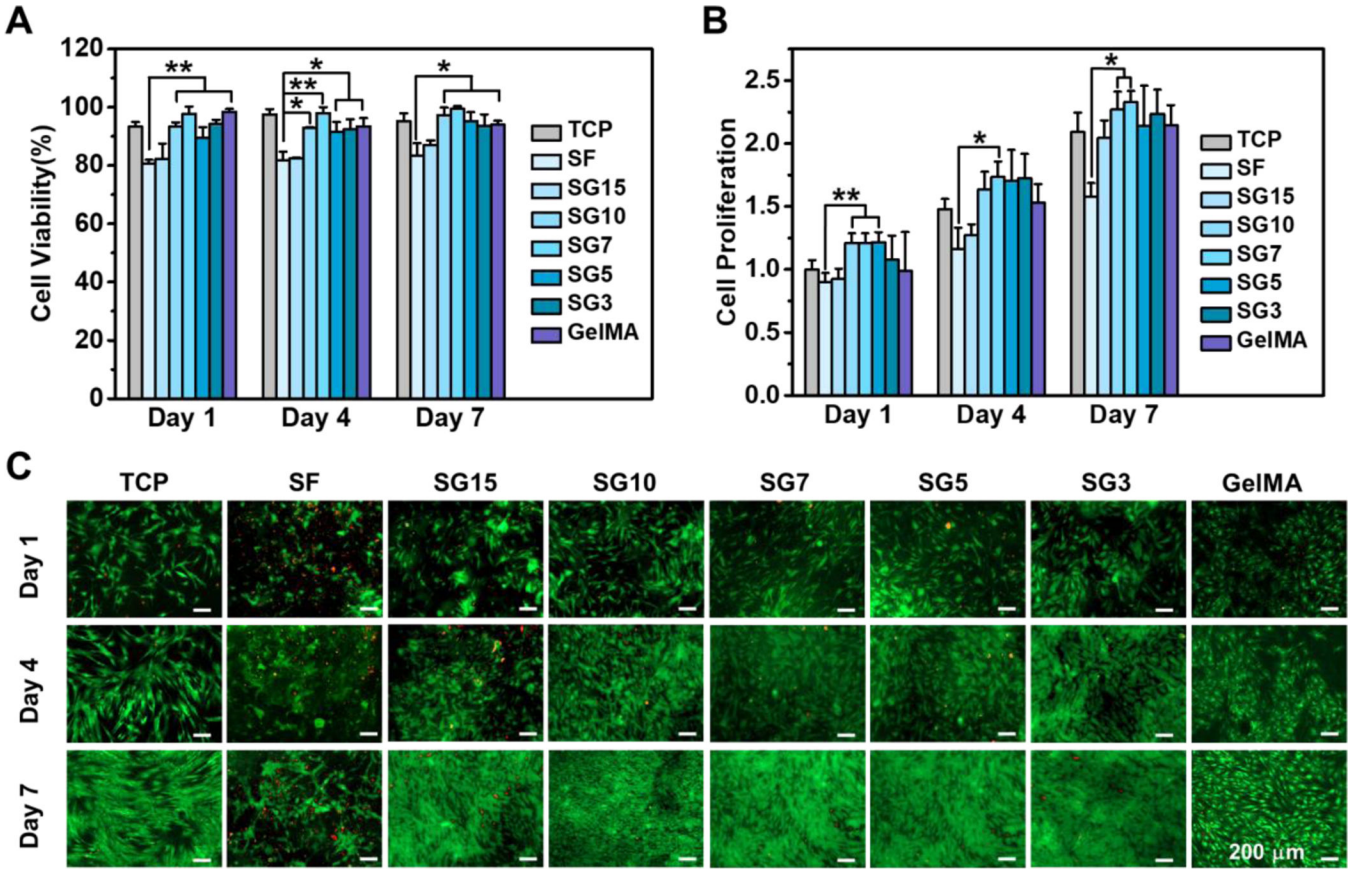

Figure 3.

In vitro biocompatibility evaluation of SG nanofibers. (A) Cell viability of MSCs grown on SF, SG and GelMA nanofibers for 1 day, 4 days and 7 days. (B) Cell proliferation behavior of MSCs incubated on SF, SG and GelMA nanofibers for 7 days. (C) Fluorescent images of MSCs cells grown on SF, SG and GelMA nanofibers. (Scale bar = 200 μm) Results are expressed as mean SD of three replicates of experiments. ANOVA (n > 3, $*p < 0.05$, $**p < 0.01$)

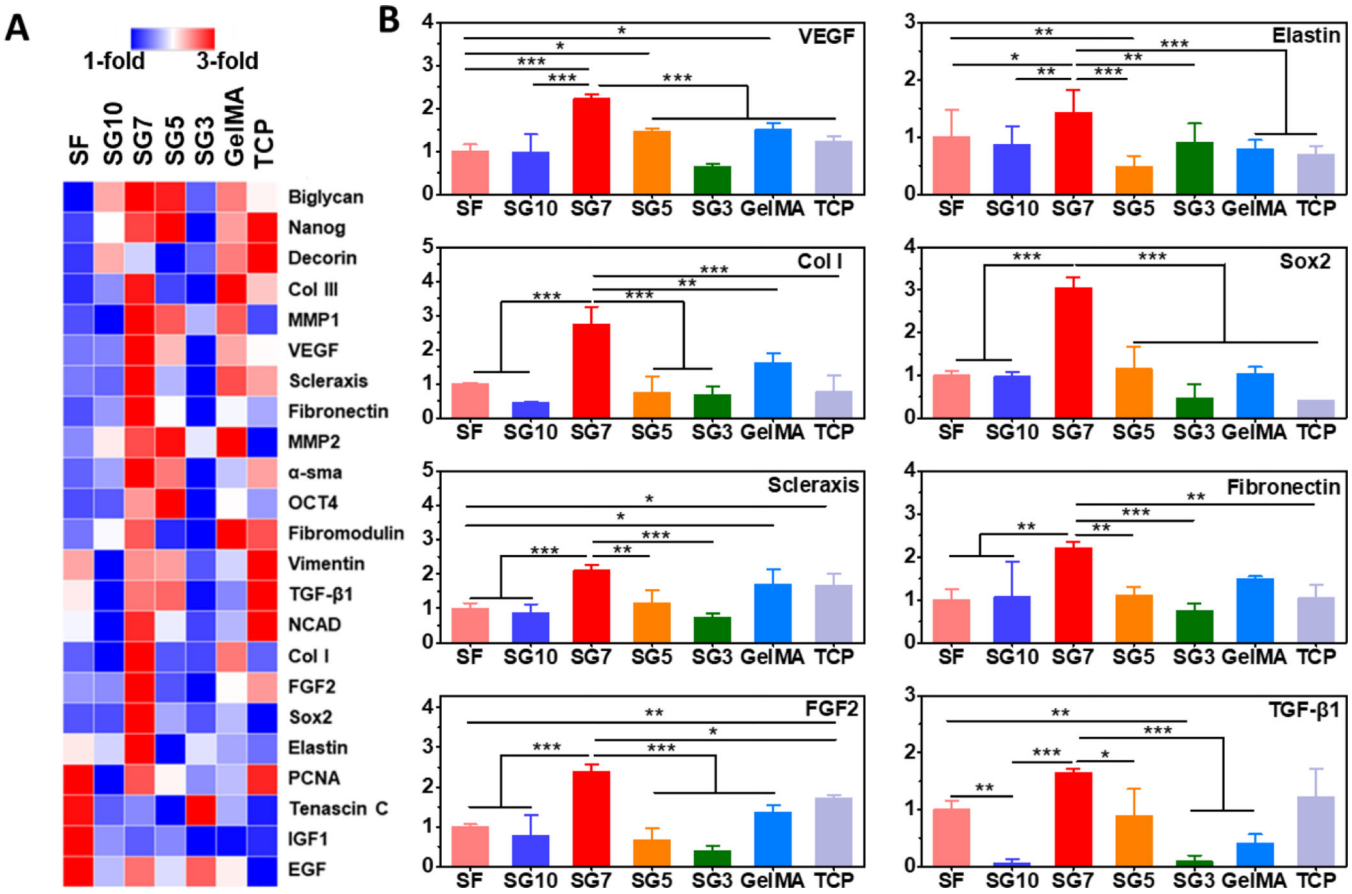

Figure 4.

Gene expression analysis of MSCs on different composition of SGs, SF and GelMA nanofibers for 7 days of culture. (A) Heatmap analysis of tenogenesis/extracellular matrix- and stemness/growth factor-related genes. (B) Quantitative analysis of gene expressions. Results are expressed as mean SD of three replicates of experiments. ANOVA ($n > 3$, $*p < 0.05$, $**p < 0.01$, $***p < 0.001$)

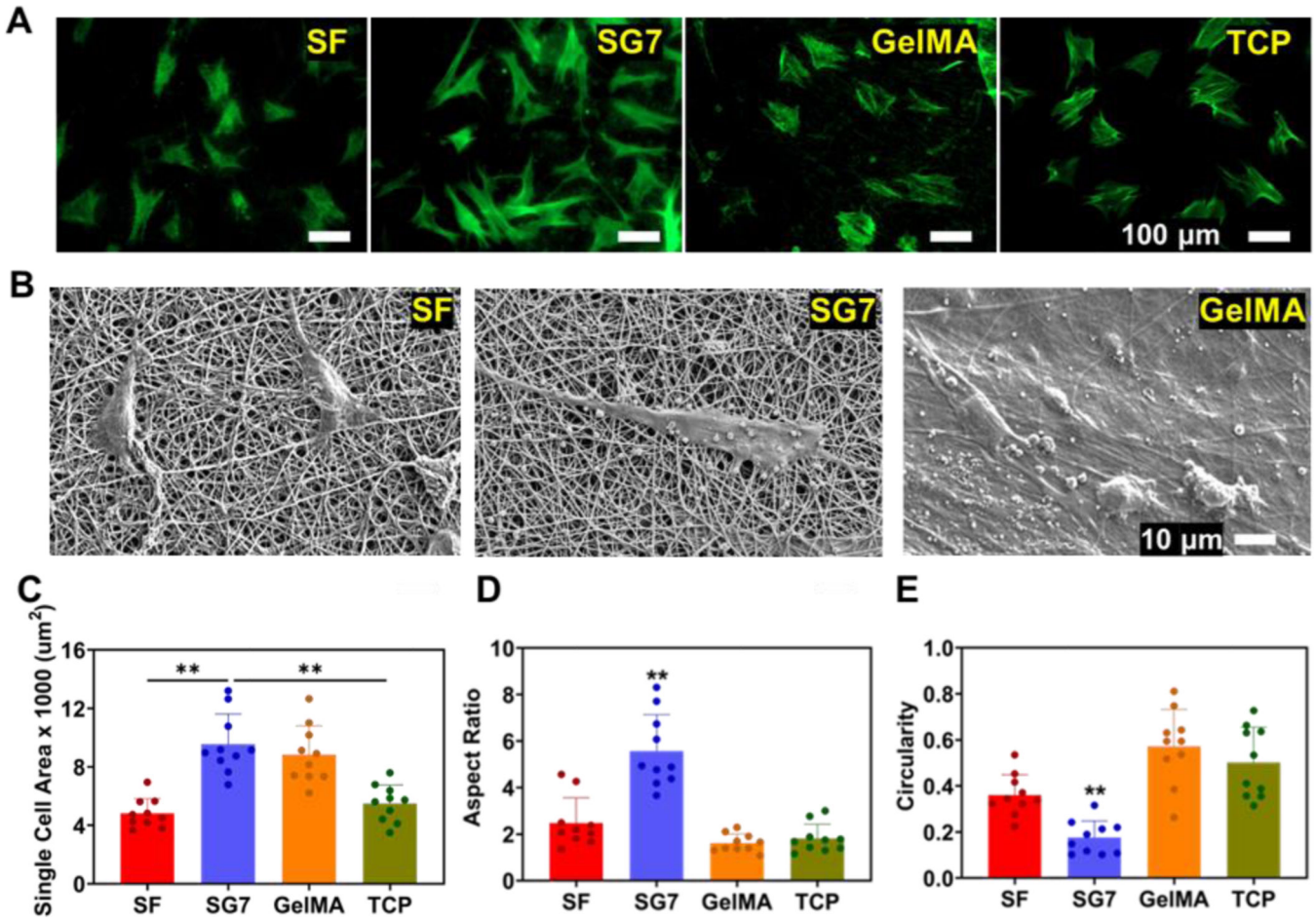

Figure 5.

The attachment behavior and morphology evaluation of MSCs cultured on SF, SG and GelMA electrospun nanofibers. (A) Fluorescent images of MSCs grown on SF, SG7 and GelMA nanofibers. (Scale bar = 100 μm) (B) SEM images of MSCs grown on SF, SG7 and GelMA nanofibers. (Scale bar = 10 μm) Quantification of (C) cell area, (D) aspect ratio and (E) circularity of the single cell. Results are expressed as mean SD of experiments. ANOVA ($n > 3$, $*p < 0.05$, $**p < 0.01$).

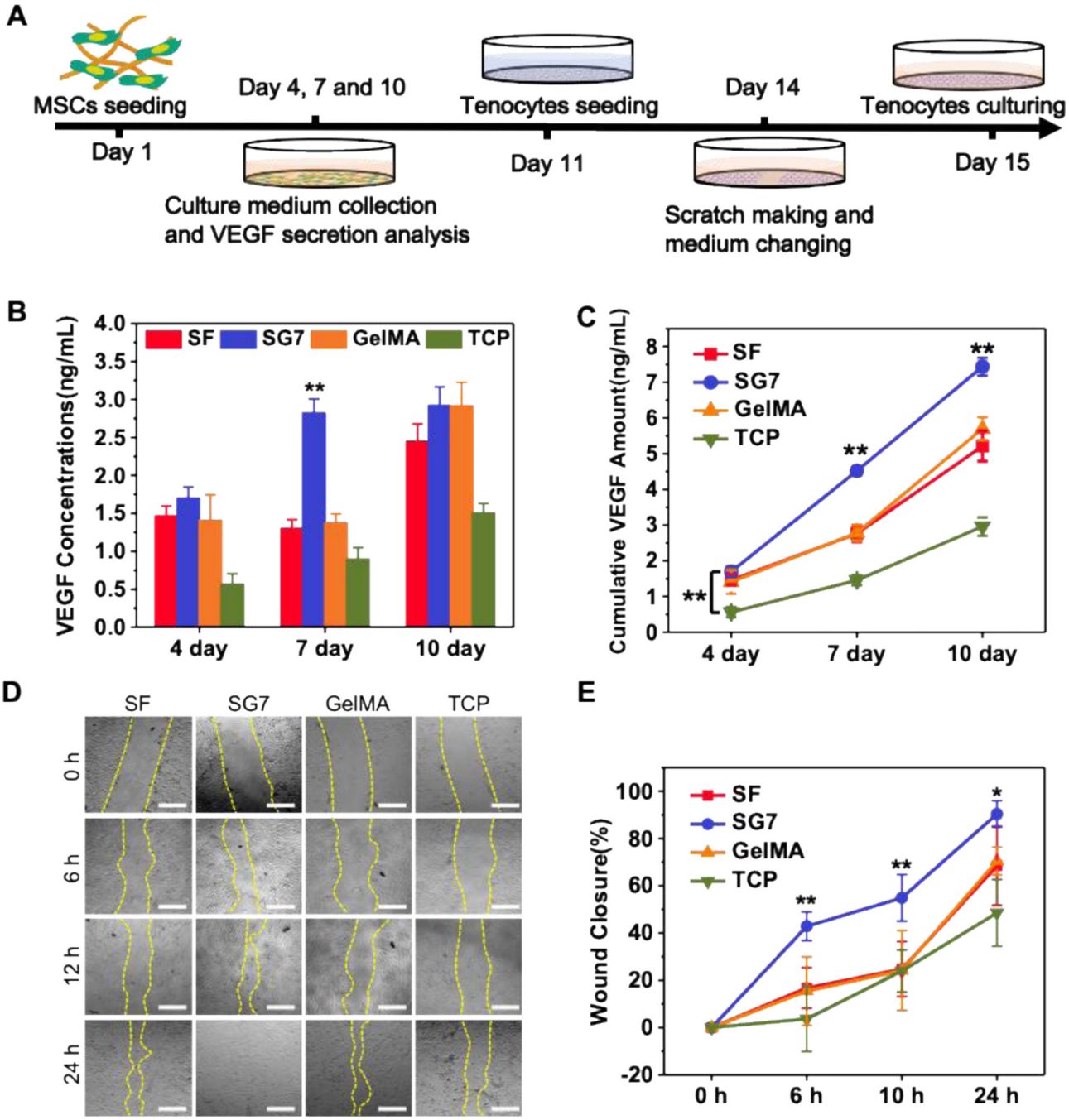

Figure 6.

Paracrine signal production behavior of MSCs and the *in vitro* tendon repair assay. (A) Timeline and schematic of VEGF secretion assay and in vitro wound healing. (B) VEGF secretion and (C) cumulative VEGF secreted amount of MSCs after cultured on SF, SG7 and GelMA nanofibers for 4 days, 7 days and 10 days. (D) Cell migration assay of tenocytes after culture with MSC-conditioned medium. (Scale bar = 500 μm) (E) Quantification of the wound closure efficacy of tenocytes based on the cell migration assay. Results are expressed as mean SD of experiments. ANOVA (n > 3, *$p < 0.05$, **$p < 0.01$)

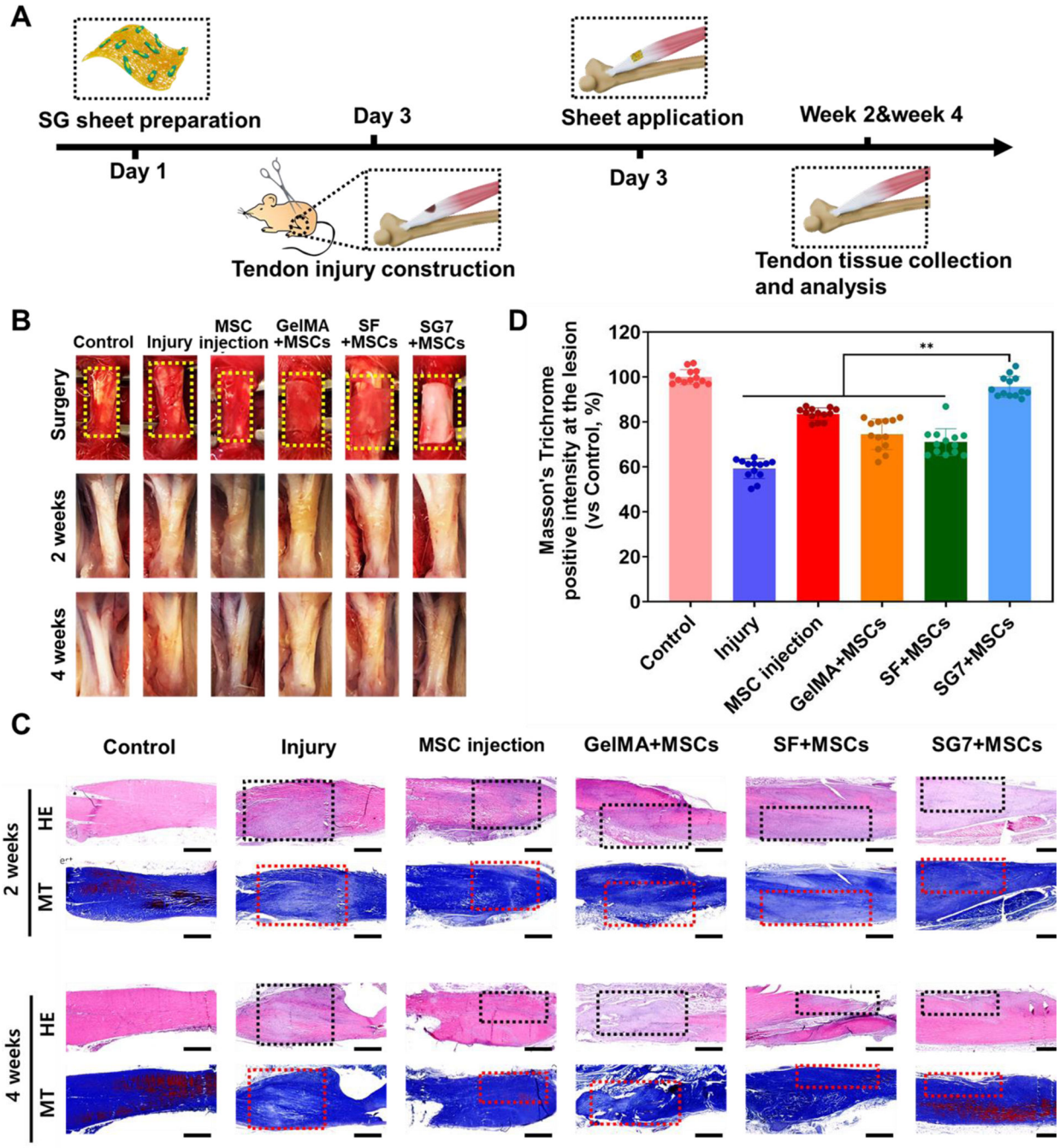

Figure 7.

In vivo tendon repair efficacy and histological analysis. (A) Timeline and schematic of in vivo tendon tissue repair experiment. (B) Images of rat's Achilles tendon after implantation. (C) H&E and Masson Trichrome staining images of tendon sections after 2 weeks and 4 weeks post-implantation. (Scale bar = 1 mm) (D) Quantitative analysis of Masson's trichrome positive intensity at lesions. Results are expressed as mean SD of experiments. ANOVA ($n > 3$, $^{**}p < 0.01$)

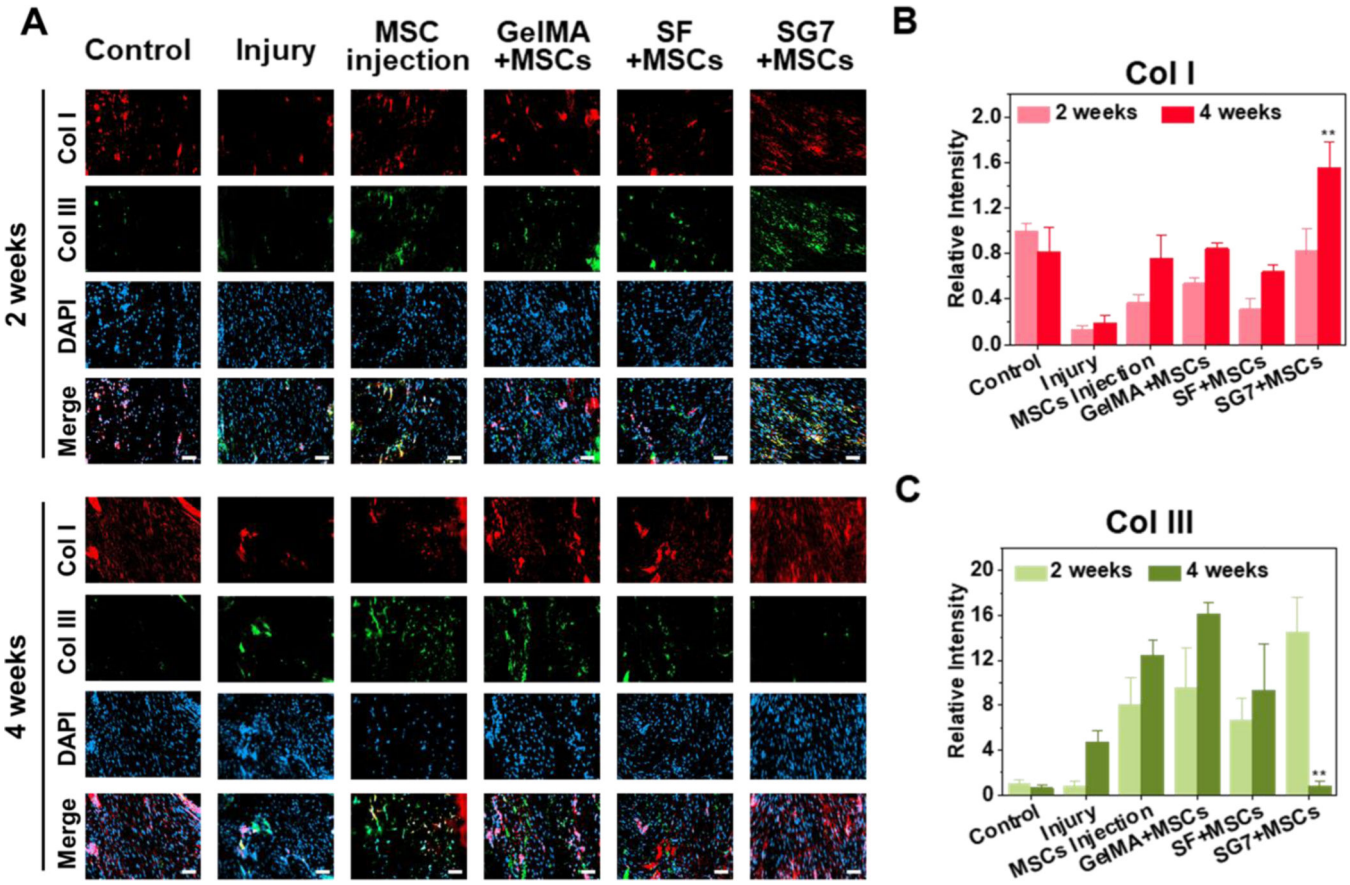

Figure 8.

Immunofluorescence analysis of tendon tissues. (A) Fluorescent images associated with the production of Col I and Col III of regenerated tendon in each group at 2 weeks and 4 weeks. (Scale bar = 50 μm) (B) Quantitative analysis of the production of Col I. (C) Quantitative analysis of the production of Col III. Results are expressed as mean SD of experiments. ANOVA (n > 3, $^{**}p < 0.01$)